Equations of state for polyamide-6 and its nanocomposites. 1. Fundamentals and the matrix

Utracki, L. A.

Publisher's version / la version de l'éditeur:
Journal of Polymer Science Part B: Polymer Physics, 47, 3, pp. 299-313, 2008-12-18

Web page / page Web
http://dx.doi.org/10.1002/polb.21640
http://nparc.cisti-icist.nrc-cnrc.gc.ca/npsi/ctrl?action=rtdoc&an=14299080&lang=en
http://nparc.cisti-icist.nrc-cnrc.gc.ca/npsi/ctrl?action=rtdoc&an=14299080&lang=fr

Equations of State for Polyamide-6 and Its Nanocomposites. 1. Fundamentals and the Matrix

L. A. UTRACKI

National Research Council Canada, Industrial Materials Institute, 75 de Mortagne, Boucherville, QC, Canada J4B 6Y4

Received 15 September 2008; revised 5 November 2008; accepted 9 November 2008
DOI: 10.1002/polb.21640
Published online in Wiley InterScience (www.interscience.wiley.com).

ABSTRACT: The pressure-volume-temperature (*PVT*) surface of polyamide-6 (PA-6) was determined in the range of temperature $T = 300$–600 K and pressure $P = 0.1$–190 MPa. The data were analyzed separately for the molten and the noncrystalline phase using the Simha-Somcynsky (S-S) equation of state (eos) based on the cell-hole theory. At $T_g(P) \leq T \leq T_m(P)$, the "solid" state comprises liquid phase with crystals dispersed in it. The *PVT* behavior of the latter phase was described using Midha-Nanda-Simha-Jain (MNSJ) eos based on the cell theory. The data fitting to these two theories yielded two sets of the Lennard-Jones interaction parameters: ε^*(S-S) $= 34.0 \pm 0.3$ and ε^*(MNSJ) $= 22.8 \pm 0.3$ kJ/mol, whereas v^*(S-S) $= 32.00 \pm 0.1$ and v^*(MNSJ) $= 27.9 \pm 0.2$ mL/mol. The raw *PVT* data were numerically differentiated to obtain the thermal expansion and compressibility coefficients, α and κ, respectively. At constant P, κ followed the same dependence on both sides of the melting zone near T_m. By contrast, $\alpha = \alpha(T)$ dependencies were dramatically different for the solid and molten phase; at $T < T_m$, α linearly increased with increasing T, then within the melting zone, its value step-wise decreased, to slowly increase at higher temperatures. ©2008 Wiley Periodicals, Inc. J Polym Sci Part B: Polym Phys 47: 299–313, 2009

Keywords: compression; compressibility coefficient; crystallization; free volume; glass transition; lattice models; melt; melting point; nanocomposites; nylon; polyamides; polyamide-6; statistical thermodynamics; thermal expansion coefficient

INTRODUCTION

Theoretical Equation of State

Any mathematical relation between pressure, P, temperature, T, and volume, V, may be called equation of state (eos)[1] Theoretical eos for macromolecular systems are based on the Lennard-Jones and Devonshire, L-JD, cell model developed for gases, and years later modified to accommodate short chain r-mer molecules.[2,3] In the model, each molecule is confined to a lattice cell, each cell is occupied, all neighboring molecules are at a distance a, and the potential energy is spherically symmetrical, given by the Lennard-Jones (L-J) 6-12 potential. Assumption of a fully packed lattice implies dense packing with crystal-like ordering of molecules. Accordingly, it has been found that eos based on the L-JD model better describes solid than liquid systems. A decade later, Peek and Hill[4] introduced unoccupied cells into a rigid lattice obtaining a complex eos that better described the *PVT* relation of liquids. The statistical thermodynamic theory of Simha and Somcynsky (S-S)[5] adopted the cell-hole lattice model, incorporating unoccupied cells or "holes" in the lattice. The theory has been most successful in describing diverse physical aspects of the molten polymeric

Correspondence to: L. A. Utracki (E-mail: leszek.utracki@cnrc-nrc.gc.ca)

Journal of Polymer Science: Part B: Polymer Physics, Vol. 47, 299–313 (2009)

systems at the thermodynamic equilibrium and under nonequilibrium conditions.[1]

For polymeric glasses at very low-temperature ($T < 80$ K), Simha et al. used a cell lattice model, deriving the Helmholtz free energy with three terms: the zero energy at $T = 0$ K, the configurational interaction energy expressed by the L-J potential, and the segments energy expressed by Einstein assembly of harmonic oscillators.[6] At the reduced temperatures $\widetilde{T} \leq 0.004$, the reduced thermal expansion coefficient, $\widetilde{\alpha} = \widetilde{\alpha}(\widetilde{T})$, of several polymers superposed on the theoretical curve, indicating existence of the corresponding states. The superposition at $T > 80$ K failed, owing to the lowest sub-T_g transition.[7] Midha and Nanda (MN) [8] adopted this model for their quantum-mechanical version of the L-JD cell theory for crystalline polymers, taking into account harmonic and anharmonic contributions to the interaction energy. The MN model was subsequently refined by Simha and Jain who demonstrated that the characteristic vibration frequency at $T = 0$ K follows from the earlier theory.[6] The resulting MNSJ version was successfully applied to several semicrystalline polymers.[9–11]

Pressure-Volume-Temperature Measurements

The pressure-volume-temperature (*PVT*) measurements are mainly performed for determining the engineering properties, namely the thermal expansion and compressibility coefficients, (α and κ, respectively):

$$\alpha \equiv (\partial \ln V/\partial T)_{T^0,P,q}; \quad \kappa \equiv (\partial \ln V/\partial P)_{T,P^0,q} \quad (1)$$

Here P^0 and T^0 are solidification pressure and temperature, respectively, and q is the rate of heating or compressing.[12] A number of eos has been proposed for molten polymer, and some have been extended to the vitreous state.[13] By contrast, a rigorous analysis of semicrystalline polymer *PVT* is difficult and rarely attempted.

This work focuses on the *PVT* behavior of poly(ε-caprolactam), PA-6, and its clay-containing nanocomposites (CPNC) in the full range of the independent variables. Direct computations of α and κ show surprisingly large difference in their behavior. The effect is particularly significant in CPNC. Comparison of the experimental data with the theoretical predictions may provide explanations for such behavior. Thus, this Part 1 provides the theoretical basis for the analysis and examines behavior of the PA-6 matrix; the Part 2 will discuss the influences of clay nanoparticles on the *PVT* behavior.

MOLTEN STATE THEORY

The S-S cell-hole theory was derived for spherical and chain molecule fluids.[5] The model lattice contains volume fraction of occupied sites, y, and that of nonoccupied sites (or holes), $h = 1–y$. From the Helmholtz free energy, F, the S-S eos was obtained:

$$\widetilde{P} \equiv -\left(\partial \widetilde{F}/\partial \widetilde{V}\right)_T \Rightarrow \widetilde{P}\widetilde{V}/\widetilde{T} = (1-U)^{-1} + 2yQ^2(AQ^2 - B)/\widetilde{T} \quad (2)$$

$$\left(\partial \widetilde{F}/\partial y\right)_{\widetilde{V}\widetilde{T}} = 0 \Rightarrow 3c\left[(U - 1/3)/(1-U) - yQ^2(3AQ^2 - 2B)/6\widetilde{T}\right] + (1-s) - s\ln[(1-y)/y] = 0 \quad (3)$$

where $Q = 1/(y\widetilde{V})$, $U = 2^{-1/6}yQ^{1/3}$, $A = 1.011$ and $B = 1.2045$ (for the face-centered cubic lattice). Equation 3 is only valid at the thermodynamic equilibrium, thus, it is not to be used for the vitreous state. The variables marked by tilde are reduced:

$$\left.\begin{array}{l} \widetilde{P} = P/P^*;\ P^* = zq\varepsilon^*/(sv^*) \\ \widetilde{T} = T/T^*;\ T^* = zq\varepsilon^*/(Rc) \\ \widetilde{V} = V/V^*;\ V^* = v^*/M_s \end{array}\right\} (P^*V^*/T^*)M_s = Rc/s \quad (4)$$

The characteristic quantities, P^*, T^*, V^*, contain the L-J interaction parameters: the maximum attractive energy, ε^*, and the segmental repulsion volume, v^*, per statistical segment. The latter is defined as $M_s = M_n/s$, where M_n is the number-average molecular weight and s is the number of macromolecular segments. The parameter $3c$ indicates the external, volume-dependent degrees of freedom; $R = 83.14$ (kbar L/K mol) is the gas constant; and $zq = s(z-2) + 2$ is the number of interchain contacts in a lattice of the coordination number z, usually taken as $z = 12$.

Equations 2–4 describe the *PVT* liquid surface, and associated with it the free volume quantity, $h = h(\widetilde{V}, \widetilde{T})$. Through T^* and V^*, the *PVT* data yield the L-J measures of interactions, ε^* and v^*, defining the minimum of the 6-12 potential. For the linear, semirigid chain molecules $3c = s + 3$ and for high molecular weight polymers where

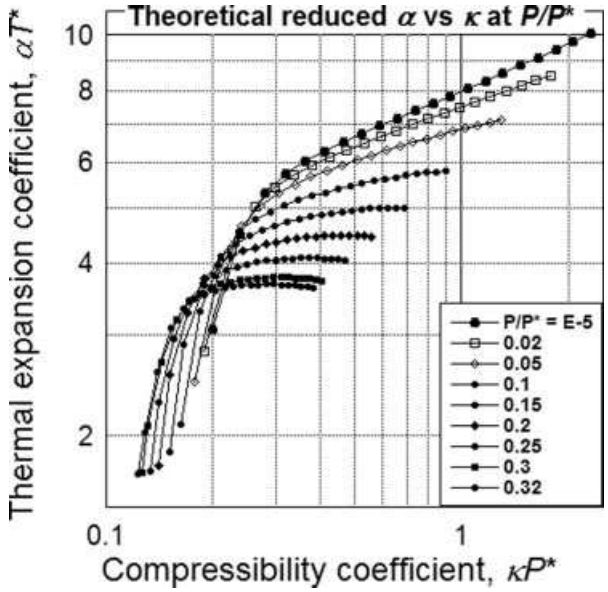

Figure 1. Melt behavior: the reduced thermal expansion coefficient as a function of the reduced compressibility at the indicated values of the reduced pressure.

$s \to \infty$, $3c/s \approx 1$. Thus, there are simple proportionalities: $\varepsilon^* \approx RT^*/30 = 2.771T^*$ and $v^* = V^*M_s$.

Considering the success of the S-S eos, it is interesting to compute the theoretical relationships between the reduced coefficients in the liquid state:

$$\tilde{\alpha} \equiv \left(\partial \ln \tilde{V}/\partial \tilde{T}\right)_{\tilde{P}}; \quad \tilde{\kappa} \equiv \left(\partial \ln \tilde{V}/\partial \tilde{P}\right)_{\tilde{T}} \qquad (1a)$$

$\tilde{\alpha} \equiv \alpha T^*$ versus $\tilde{\kappa} \equiv \kappa P^*$, as well how they vary with the hole fraction, h (proportional to T). The computations were carried within the full range of the reduced variables following the described procedure.[14] The resulting dependencies in Figures 1 and 2 are valid under the condition of thermodynamic equilibrium. Contrary to what one may have expected, $\tilde{\kappa}$ and $\tilde{\alpha}$, differently vary with the measure of free volume, h. For dense fluids, compressibility is small, slightly varying with P, whereas the thermal expansion coefficient changes significantly, especially at low P. The experimental data of α versus κ of molten polystyrene (PS) confirmed the S-S eos predictions.

THEORIES OF SOLID POLYMERS

The thermodynamics of crystalline substances (including polymers) have been considered either basing on the Grüneisen parameter, γ_G, or deriving the statistical thermodynamic lattice theory of solid polymers. The Grüneisen dimensionless parameter was originally defined as a density gradient of the crystalline lattice frequency, ν[15]:

$$\gamma_G = -(\partial \ln \nu/\partial \ln V)_P \qquad (5a)$$

while the macroscopic scale parameter is usually expressed as:

$$\gamma_G \cong \alpha V/\kappa C_P \qquad (5b)$$

In eq 5b, V, α, κ, and C_P are respectively, the specific volume, thermal expansion coefficient, compressibility coefficient, and heat capacity at constant pressure. The advantage and utility of eq 5b rests in the interrelation between measurable quantities and their derivatives, for example, expressing compressibility in terms of the bulk, B, or tensile, E, modulus.

Fundamentally, at very low temperatures, one may expect constant value of γ_G, as here, the crystal behavior is dominated by the quantum interactions and small changes of the specific volume, without transitions. The model computations of the lattice Grüneisen parameter for n-alkanes indicated that γ_G increases with T and chain length. Experimental examinations of γ_G constancy under constant T and P (usually under the ambient conditions) have been carried out. Thus, Barker reported that at room temperature, 68

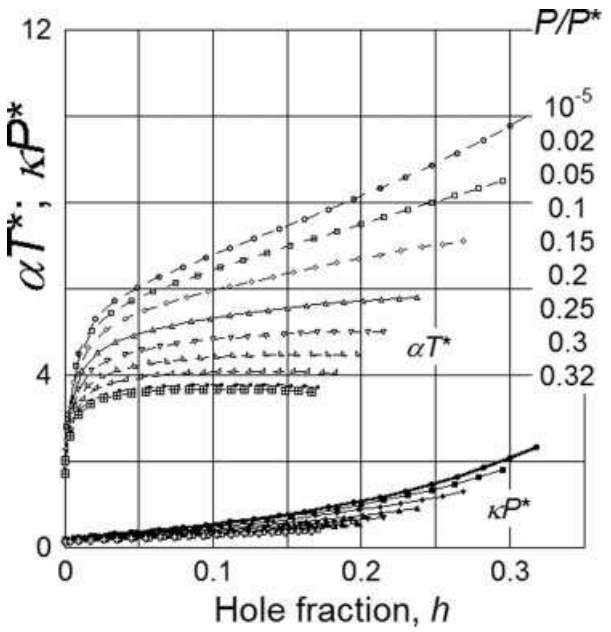

Figure 2. Melt behavior: the reduced thermal expansion and reduced compressibility coefficients as a function of the hole fraction at the indicated reduced pressures.

materials, ranging from metals to polymers, have a nearly constant value of the product: $\alpha^2 E = 140 s_p$ [N/(m K)^2] (s_p is a dimensionless spread factor, $0.5 < s_p < 2$).[16,17] Wada et al. calculated from the pressure dependence of ultrasonic velocity $\gamma_G \approx 4 \pm 0.2$ for glassy and semicrystalline polymers.[18] Comparable values of $\gamma_G \approx 6 \pm 1$ were calculated for hydrocarbons ideal crystals at $T = 300$ K and $P = 1$ bar.[19] Calculation of γ_G for polymers from the bulk modulus gave much larger values: $\gamma_G \approx 25 \pm 4$.[20] On the other hand, for a series of polyamides at room temperature, eq 5b gave: $\gamma_G = 0.45$ to 0.64.[14] Its magnitude was found increasing with T and decreases with P.[21–23] The diversity of Grüneisen parameter values originates from the applied methods of measurements, calculation procedures, and extension of the original concept to polyatomic substances having a variety of morphologies.

Pastine analyzed the *PVT* behavior of semicrystalline polyethylene, PE, by assuming additivity of behavior for crystalline with that of amorphous domains, that is, knowing the degree of crystallinity and eos of the two phases he calculated the relation: $V = V(T)$ at $P = \text{const}$.[24] He obtained a reasonable agreement with the experimental data at $T = 298$ but not at 373 K, caused by the pressure-induced crystallinity increases. His following paper focused on the thermal expansion of semicrystalline polymers written as a function of V, T and the degree of crystallinity, X_{cryst}.[25] The idea that at constant P, the specific volume of semicrystalline polymers, $V = V(T)$, is an additive property of the amorphous and crystalline phase seems logical and worth pursuing.

Following the harmonic approximation by Simha et al.,[6] Midha and Nanda derived eos for the crystalline polymers.[8] Their basic assumption was that the lattice cell model with L-J 6-12 potential and first order anharmonics well represents the ordered crystalline structure. Next, Simha and Jain in a series of papers modified the theory, for example, deriving an expression for the characteristic frequency, ν_0.[9–11] Consequently, the crystalline state eos has five characteristic parameters: P^*, T^*, V^*, and c/s defined in eq 4 as well as the characteristic frequency function:

$$\tilde{\theta}_0(\nu_0) \equiv h\nu_0/kT^* = 4.794 \times 10^{-11}\nu_0/T^* = 13.189(c/s)V_0^{-4/3}\frac{(A_1/2V_0^2 - B_1)^{1/2}}{M_0^{5/6}\sqrt{T^*}\sqrt[3]{V^*}} \quad (6)$$

calculable from Simha and Jain expression. Because $3c/s = 1$ offers good approximation, only the P^*, T^*, V^* parameters need to be determined by fitting the experimental data $P = P(V, T)$ to the theory. It is noteworthy that because different theories are used for description of the molten and crystalline state, respectively, different values of the ε^* and v^* parameters are expected. The MNSJ eos for crystalline solids in reduced variables is[8]:

$$\tilde{P}\tilde{V} = \left(2/\tilde{V}^2\right)\left[\left(A/\tilde{V}^2\right) - B\right] + 3\gamma_G F_1(\tilde{\theta}, \tilde{T}) - (9s/4c)ab\tilde{V}^2\tilde{\theta}'^2\left[\frac{1}{2} + \frac{2X}{(X-1)^2}\right] + (9s/8c)\gamma_G b\tilde{V}^2\tilde{\theta}'^2\left[\frac{1}{2} + \frac{3X+1}{(X-1)^2} - (\tilde{\theta}/\tilde{T})\frac{X(3+X)}{(X-1)^3}\right] \quad (7a)$$

The secondary functions in eq 7a are defined as:

$$\gamma_{G,0} = -(\partial \ln v_0/\partial \ln V)_T = 4/3 + A_1/(A_1 - 2B_1V^2)$$

$$\gamma_G = \gamma_{G,0}\left\{1 - (s/2c)b\tilde{V}^2\left[F_1(\tilde{\theta}_0, \tilde{T}) - (\tilde{\theta}_0^2/\tilde{T})\frac{X_0}{(X_0-1)^2}\right]\right\} - (s/c)ab\tilde{V}^2F_1(\tilde{\theta}_0, \tilde{T})$$

$$X(\tilde{\theta}, \tilde{T}) = \exp\left\{\tilde{\theta}/\tilde{T}\right\}$$

$$F_1(\tilde{\theta}, \tilde{T}) = \tilde{\theta}\left[\frac{1}{2} + \frac{1}{X-1}\right]$$

$$Y = (3s/8c)(\tilde{\theta}_0/\tilde{\theta}')^2(\tilde{\theta}_0\tilde{V})^2 b/\tilde{T}$$

$$\tilde{\theta} = \tilde{\theta}'\left[1 + (3s/8c)b\tilde{V}^2\tilde{\theta}'\right];$$

$$\tilde{\theta}' = \tilde{\theta}_0\left[1 + \left(4\tilde{T}/3\tilde{\theta}_0^2\right)F_1\left(\tilde{\theta}_0, \tilde{T}\right)Y\right] + 0(Y)$$

$$a = 1 - \frac{A_2}{\left[A_2 - 2B_2\tilde{V}^2\right]} + \frac{2A_1}{\left[A_1 - 2B_1\tilde{V}^2\right]};$$

$$b = \left[\left(A_2/\tilde{V}^2\right) - 2B_2\right]/\left[\left(A_1/\tilde{V}^2\right) - 2B_1\right]^2 \quad (7b)$$

In the above equations, the additional lattice constants are: $A_1 = 22.1060$, $B_1 = 5.2797$, $A_2 = 200.653$, and $B_2 = 14.334$.

The logical sequence of calculations requires that first the melts data are fitted to S-S eos, eqs 2–4, giving the characteristic parameters: P^*, T^*, V^*. Next, the specific volume of the liquid polymer at $T < T_m$ may be calculated. In parallel, following Simha and Jain procedure, the approximate values of the reducing parameters and θ_0 may be

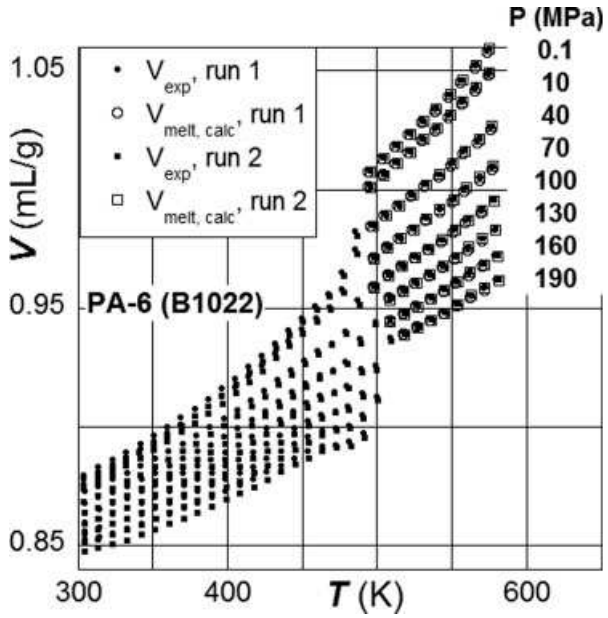

Figure 3. The *PVT* dependence of PA-6. Note the excellent superposition of data (solid symbols) from two runs in the semicrystalline and molten phase; T_m(PA-6) = 493 ± 2 K. Computed from eqs 2–4 behavior in the melt is shown by open symbols.

computed. By contrast with Pastine's procedure, the apparent degree of crystallinity at $T < T_m$ is taken as an adjustable parameter to be determined by the iterative fit of solid state data to eqs 6–8. In this Part 1 article, the calculation will be limited to PA-6 matrix. The analysis of the multicomponent CPNC systems, the analysis will be reported in Part 2.

EXPERIMENTAL

The PA-6 1022B was obtained through the courtesy of Dr. Arimitsu Usuki (Toyota R and D Labs). The weight-average molecular weight of the matrix polymer, PA-6, was $M_w \approx 22$ kg/mol.

The *PVT* behavior was studied using a Gnomix pressure dilatometer (Gnomix, Boulder, Colorado), within the range: T = 300–600 K and P = 0.1–190 MPa. The molten state was observed at $T \geq 520$ K. Prior to testing, the material was dried under vacuum for 48 h at 80 °C. The absolute value of V at ambient conditions was determined (in a glove compartment under positive pressure of dry N_2) by the immersion method with the accuracy of $\Delta V \leq \pm 0.001$ mL/g.[26] Next, the dried pellets were loaded into the dilatometer, pressurized to 10 MPa, premolded at $T \geq 130$ °C for 10 min, and then cooled to ~ 30 °C at a rate of 2.5 °C/min. For each sample, two to six runs were carried out following the "standard" isothermal scan, starting at the lowest temperature, T = 300 K, and measuring $\Delta V = V(P)$ at ΔP = 30 MPa intervals, then increasing T by 10 °C and repeating the pressurization steps. Thus, in the "standard" runs, the specimen is exposed to the highest T = 600 K only once, reducing a possibility of thermal degradation. The average error in V was ≤ 0.03%. There was no attempt to control the samples crystallinity by annealing. The total run time ranged from 23 to 45 h.

Examples of the observed dependencies are presented in Figures 3 and 4 as $V = V(P, T)$. The former Figure presents reproducible data from two runs (filled symbols) as well as the goodness of fit of eqs 2–4 within the molten region (empty symbols). The range of the independent variables extended from below the glass transition temperature, T_g(PA-6) ≤ 323 K, to well above T_m(PA-6) ≈ 500 K. For calculation of α and κ coefficients, the *PVT* data need to be plotted as isobars or isotherms of ln$V$ versus T or P, respectively. Because the experimental isobaric tests involved adiabatic heating, the data had to be interpolated to constant T (see Fig. 4). The interpolation was carried out assuming linear volume changes between two adjacent data points.

In addition to pressure dilatometry, the differential scanning calorimetry (DSC) measurements were conducted at T = 30 to 250 °C, scans rates:

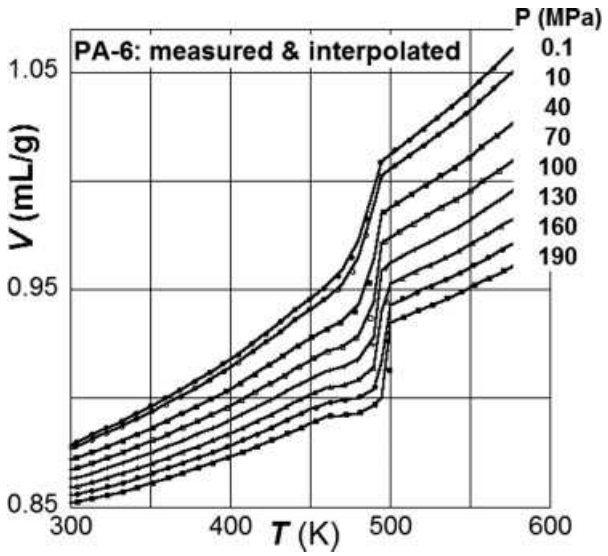

Figure 4. Specific volume, V, versus T at P = 0.1–190 MPa for PA-6; experimental data (lines) and interpolated to constant-T ones (points).

2, 6, and 20 °C/min, first heating, then cooling down, and reheating, with 2 min pause between the runs. The dynamic flow behavior of 1022B PA-6 resin was also evaluated at 240 °C. The standard three sets of tests were carried out: time, strain, and frequency sweeps.[27]

RESULTS

The Molten State

The molten *PVT* data were computer-fitted to eqs 2 and 3 using the MicroMath least squares protocol. The results are summarized in Table 1. The goodness of fit was excellent, as evidenced by three statistical measures: r^2, σ, and *CD*. The characteristic parameters of this PA-6 slightly differ from those determined for PA-6 1015B from Ube having lower molecular weight.[28,29] The difference may originate in different molecular weight and/or the molecular structure. In consequence, the bulk-averaged L-J parameters from eq 4 are also different. The molecular weight dependence of the characteristic parameters and L-J quantities was reported for PS.[30] It is noteworthy that the larger value of T^* for 1022B means that in this polymer the free volume content (at the same P and T) is smaller than that in 1015B[13]; this could be expected for higher molecular weight.

The Melting Region

Figures 3 and 4 show a wide melting region near $T \approx 500$ K. Figure 5 defines three parameters that characterize the region: the melting temperature, T_m, the width of the transition, ΔT_m, and the volume change, ΔV_m. Their pressure dependencies are displayed in Figure 6.

Table 1. Statistics of Fitting the eos to Experimental Data and the Computed Parameters of Two PA-6 Resins: 1015B (From refs. 28 and 29) and the Present Measurements of 1022B

Parameter	1015B	1022B
Correlation coefficient squared (r^2)	0.999999	0.999998
Standard deviation of data (σ)	0.00112	0.00127
Coefficient of determination (CD)	0.998602	0.998328
P^* (bar)	12574 ± 82	10675 ± 116
T^* (K)	11134 ± 32	12282 ± 66
$V^* \times 10^4$ (mL/g)	8919.3 ± 9.6	9198.0 ± 16
M_s (g/mol)	27.51 ± 0.29	34.66 ± 0.6
ε^* (kJ/mol)	31.23 ± 0.09	34.05 ± 0.30
v^* (mL/mol)	24.54 ± 0.03	32.00 ± 0.05

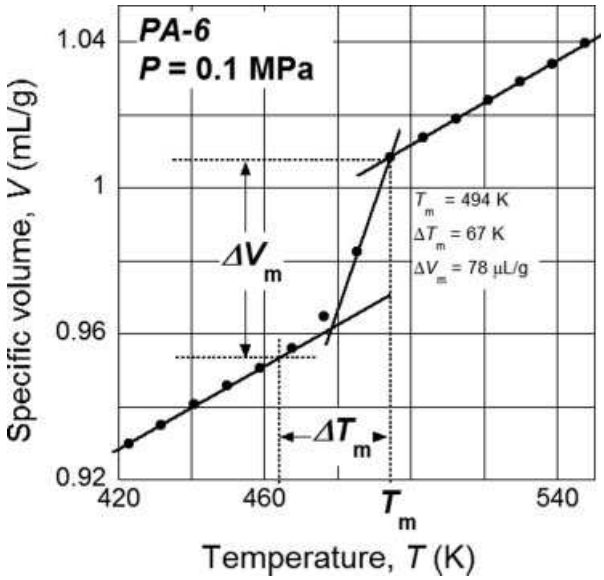

Figure 5. Definition of the three parameters of the melting zone.

Solid State Region at $T < T_m$

The crystalline region between the melting point and the glass transition, $T_g \leq T \leq T_m$, is of particular interest. The system may be treated as slurry of crystals in molten matrix. Thus, the thermodynamic interpretation of this region is complicated; the volume change of the liquid phase depends on

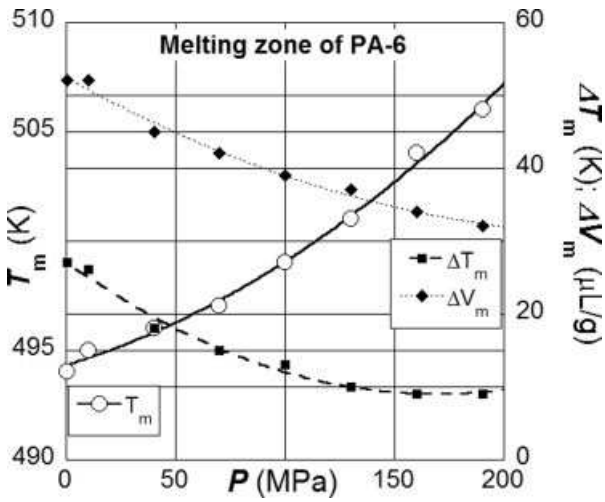

Figure 6. Pressure dependence of the melting zone parameters for PA-6 (1022B).

that of the free volume, whereas that of the crystals is controlled by the anharmonic vibration of covalently bonded atoms and by the intermolecular local free volume interactions between chains.[31] Furthermore, the morphology (as represented by the helix structure and crystalline content) changes with the time (t), T and P. Many polymers are known to change crystallographic form and/or shrink axially when heated.[32–35] The XRD, FTIR, and Raman data show that while the crystals shrink in the longitudinal direction, their skeletal length increased with T.

The T_g of polyamides depends on crystallinity, crystalline form, draw-down ratio, and relative humidity (in wt%). Thus, for PA-6, Khanna et al. found that: $T_g \approx 326–0.168w–6.208\sqrt{w}$.[36,37] The most often cited value for dry PA-6 is $T_g \approx 327$ K.[38,39] Furthermore, T_g depends on the residual stresses and annealing.[40] In the present case, T_g was difficult to detect as the starting temperature for PVT measurements (30 °C) was close to the transition. In addition, it is known that for semicrystalline polymers, the relatively small change of specific volume at T_g is difficult to detect on the PVT surface. Thus, two methods were used for estimating T_g versus P dependency: (1) the change of slope in the thermal expansion coefficient using α versus T isobaric plots; and (2) by plotting the difference between experimental data and polynomial fit as function of T. The results were comparable, indicating that for PA-6 at ambient pressure $T_g = 316 \pm 2$ K and the pressure gradient, $dT_g/dP = 0.107$ K/MPa. According to Khanna et al. equation, the relative humidity of 1.55% might account for the observed 11 K difference in T_g.

$V = V(P, T)$ in Crystalline PA-6 Region at $T_g \leq T \leq T_m$

The experimental PVT values at $T = 300–500$ K were least squares fitted to MNSJ eqs 6–8 using MicroMath. The initial parameter values were calculated following the Simha and Jain procedure[9] as: $P^* = 5531$ MPa, $T^* = 10{,}349$ K, $V^* = 0.8804$ mL/g, thus $\theta_0 = 0.05$. The least squares iterative fit to data gave: $P^* = 8161$ MPa, $T^* = 8226$ K, $V^* = 0.91087$ mL/g and $\theta_0 = 0.0200$. The reason for the change is evident in Figure 7—the theoretical curves predicted by the MNSJ theory are nearly linear, whereas the measured performance of PA-6 follows second-order dependence. The minimization of error results in crossing the one set of curves by another at $T \approx 420$ K. The error is especially large at ambient pressure, progressively decreasing with P.

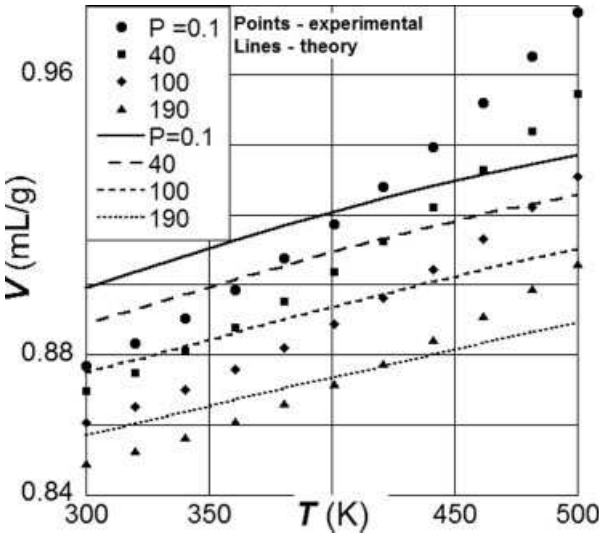

Figure 7. Temperature dependence of specific volume, V, for PA-6 (1022B) at $P = 0.1$, 40, 100, and 190 MPa; points—experimental, lines computed from MNSJ theory.

Differential Scanning Calorimetry

Before pursuing discussion on the PVT behavior in the crystalline region, it is interesting to consider the differential scanning calorimetry (DSC) results summarized in Table 2. The crystalline content at the first heating is the most important. The zero-scanning rate results (at 0 °C/min) were calculated by polynomial fit of data obtained at the scanning rates of 2, 6, and 20 °C/min. Crystallinity was calculated from the heat of melting value: ΔH_m(crystal) = 230 (J/g).[41]

DISCUSSION

In this article, the PVT behavior of PA-6 was analyzed in the full range of experimental variables, starting in the glass-crystal region, then moving to melt-crystal state, and finally to the molten state. The thermodynamic analysis of data was conducted in the opposite direction, starting with the molten phase where the S-S hole-cell equilibrium thermodynamic theory is valid. Next, the melting region was described by three parameters: the melting point, the width of the melting zone and the volume increase upon melting. The crystalline region at $T_g \leq T \leq T_m$, was analyzed using the MNSJ cell theory. The glass transition

Table 2. DSC Results for PA-6 at Three Scanning Rates

No.	Property	Scan Rate (°C/min) 0	2	6	20
1	1st heating; glass transition T_g (K)	316.1	316.1		
	Melting zone ΔT_m (K)	48.0	50.0	37.4	30.7
	Melting points T_m (K)	495.1	495.1	495.1	495.1
	Heat of melting ΔH_m (J/g)	89	90.7	86.7	89.6
	Crystallinity X_{cryst} (%)	39.0	39.4	37.7	39.0
2	Cooling down				
	Crystallization zone ΔT_m (K)	27.0	28.6	34.4	50.2
	Crystallization temp. T_c (K)	452.1	451.1	441.1	425.1
	Heat of crystallization ΔH_m (J/g)	57.0	57.5	53.7	50.0
	Crystallinity X_{cryst} (%)	25.0	25.0	23.3	21.7
3	2nd heating: T_g (K)	315.1	315.1		
	Melting zone ΔT_m(K)	21.0	23.7	27.4	43.0
	Melting points T_m (K)	494.1	494.1	493.1	486.1; 494.1
	Heat of melting ΔH_m (J/g)	49.0	50.8	53.0	63.1
	Crystallinity X_{cryst} (%)	21.0	22.1	23.0	27.4

Notes: Crystallinity was calculated taking ΔH_m(crystal) = 230 (J/g).[41]

temperature, $T_g = 316 \pm 2$ K was detected only in low pressure *PVT* data and in the DSC scans at ambient pressure. The sub-T_g solid state region was too narrow to warrant analysis.

The Molten State

Table 1 lists the statistical parameters of the simultaneous fit of the S-S eos to the full set of the *PVT* experimental data at $T > T_m$. For comparison, the earlier results for PA-6 with lower molecular weight are also shown. It is evident that increased molecular weight and possibly change of molecular configuration resulted in higher values of L-J interaction coefficients, ε^* and v^*; for PS, these coefficients linearly increased with logarithm of M_w.[30] The dynamic shear behavior of 1022B is also different than that from that of 1015B.[27] For example, the reported strong polycondensation at 513 K for 1015B was found to be greatly reduced for 1022B, possibly because of high molecular weight.

The Melting Region

Linear macromolecules form regular helices, which expand as T increases, becoming progressively more disturbed. It is known that helix thermal expansion differs in the axial and normal directions. Furthermore, the process takes place in two T-steps, each at the specific, characteristic for each polymer temperature. [42]

For PA-6, these temperatures are about 200 and 400 K, the latter close to the Brill $\alpha \rightarrow \gamma$ phase transition at T = 390–420 K.[43,44] The melting points of these two forms are: $T_m(\alpha) = 494$ and $T_m(\gamma) = 486$ K, respectively.[45] This observation is supported by the reported effects of P on crystallinity (measured by the X-ray diffraction, XRD) during isobaric cooling at 2 K/min, from $T_m + 20$.[46] The initial crystallinity of PA-6 increased with P up to first maximum, $P_{max,1}$ dependent on molecular weight, decreased to the first minimum at $P_{min,1} \approx 130$ MPa, increased to the second maximum at $P_{max,2} \approx 160$ MPa, and then started to decrease continuously. The interpretation was based on the nonlinear effect of P on the flexibility and mobility of the structural units. However, the effect of P during isobaric crystallization might not take place during the "standard" *PVT* tests, where solid polymer is isothermally compressed to the highest pressure, then temperature increased, and compression restarted. Because of annealing during slow *PVT* measurements, the repetitive compression/decompression at increasing T and P, the crystallinity should initially increase, but as T approaches T_m, it must decrease within the premelting region.[47]

The three characteristic parameters defined in Figure 5 are displayed in Figure 6; T_m increases with P whereas ΔT_m *and* ΔV_m, decrease:

$$T_m\ (\mathrm{K}) = 494.3 + 0.0306P + 0.0001687P^2;\quad r = 0.998$$
$$\Delta T_m\ (\mathrm{K}) = 27.09 - 0.2136P + 0.0006289P^2;\quad r = 0.994$$
$$\Delta V_m\ (\mu\mathrm{l/g}) = 52.38 - 0.1668P + 0.0003234P^2;\quad r = 0.995 \qquad (9)$$

Kojima et al. studied the P-dependence of T_m of low molecular weight PA-6 at pressures up to P = 1 GPa in a high-pressure differential thermal analysis (HP-DTA) instrument.[48] The results followed the second order polynomial: T_m (K) = 499.5 + 0.2057P – 0.0000676P^2 with r^2 = 0.999. Although the T_m values are not too far apart, the averaged pressure gradient for 1022B, $dT_m/dP \approx$ 0.0616, is about 3-fold smaller.

The Crystalline Region

The DSC data in Table 2 indicate that for the studied PA-6 T_g = 316 K and T_m = 495 K. For the first heating, the melting zone started at $T \approx$ 450 K, and its width was ΔT_m = 48 K. The PA-6 crystallization resulted in crystalline content $X_{cryst} \approx$ 39% mainly of the stable α-form. The second melting had narrower melting zone (ΔT_m = 27–21 K), reduced crystallinity, $X_{cryst} \approx$ 21–30%, and it produced mixed α, γ-crystals with T_m = 486.1 and 494.1 K.

Khanna and Kuhn forcefully argued that the common method for the evaluation of PA-6 X_{cryst} from DSC leads to too high values, that is, the standard method gives X_{cryst} = 15 wt %, whereas the proposed by them method yields 3 wt %.[36] Because the DSC analysis used in this work was standard, the values of X_{cryst} are probably too high. Thus, at $T \approx$ 300–450 K, the solid phase contains > 60% of noncrystalline PA-6. Accordingly, two sets of specific volumes need to be computed: the specific volume of the crystalline phase, V_{solid}, and that of the molten PA-6, V_{melt}. It should be stressed that V_{solid} is made of variable content of PA-6 crystalline forms, viz. α, α', β, γ, and δ existing at different T and P.[34,44,49] The computations of V_{solid} and V_{melt} were carried out using the simulation subroutine of the MicroMath for $T \leq T_m$ and full range of P.

The V_{melt} values were computed from eqs 2–4 with P^*, T^*, V^* from Table 1, whereas for the crystalline phase, eqs 6–8 gave P^* = 8161 MPa, T^* = 8226 K, V^* = 0.91087 mL/g. It is noteworthy that use of the cell-hole for the liquid and the cell theory for solid phase leads to two sets of the characteristic reducing parameters: ε^*(S-S) = 34.0 ± 0.3 and ε^*(MNSJ) = 22.8 ± 0.3 kJ/mol, whereas v^*(S-S) = 32.00 ± 0.1 and v^*(MNSJ) = 27.9 ± 0.2 mL/mol, that is, the MNSJ parameters are smaller by about 10 and 30%, respectively.

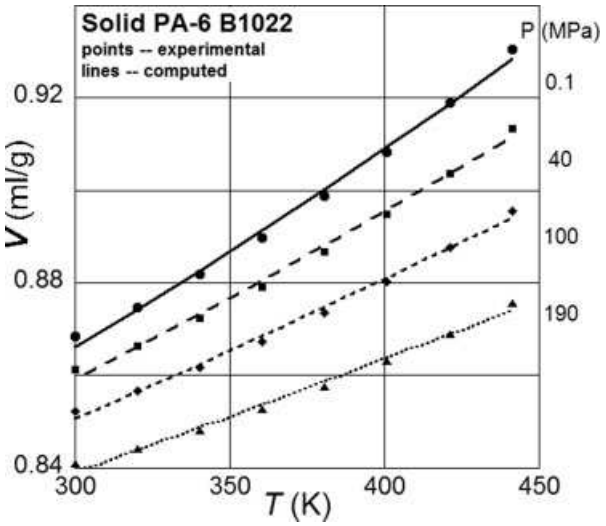

Figure 8. Temperature dependence of specific volume, V, for PA-6 (1022B) at P = 0.1, 40, 100, and 190 MPa; points–experimental, lines–computed from eq 10.

In the final iterative fit, the experimental specific volume, V, was fitted to the expression:

$$V = \Delta V_{m.c} + X_{cryst}V_{solid} + (1 - X_{cryst})V_{melt} \qquad (10)$$

were $\Delta V_{m,c}$ and X_{cryst} are treated as iteration parameters. The results are displayed in Figure 8. The values of $\Delta V_{m,c}$ and X_{cryst} at four P-levels are listed in Table 3 and shown in Figure 9. As P increases from ambient to 190 MPa the initial crystallinity $X_{cryst}(P = 0.1)$ = 15-wt % nearly doubles with the initial gradient of $dX_{cryst}/dP \approx$ 0.21 (%/MPa). By comparison, calculated from Gogolewski and Pennings data, the ambient pressure crystallinity of PA-6 $X_{cryst}(P = 0.1)$ = 25 wt %, and the maximum gradient at $P \approx$ 500 MPa was $dX/dP \approx$ 0.42 (%/MPa).[49] The equilibrium crystalline content in PA-6 at ambient pressure has been cited as X_{cryst} = 29–31%.[50–52] thus the lower value extracted from the initial *PVT* data indicates a partial crystallinity. During the *PVT* tests, as T and P increase, the polymer anneals toward equilibrium. The maximum crystallization rate is

Table 3. Crystallinity and the Volume Change by Annealing During PVT Testing

Parameter\Pressure, P (MPa)	0.1	40	100	190
Correlation coefficient squared (r^2)	0.999998	0.999998	0.999998	0.999999
Standard deviation of data (σ)	0.00158	0.00144	0.00123	0.00113
Coefficient of determination (CD)	0.995	0.997	0.994	0.993
X_{cryst} (wt%)	14.8 ± 4.3	24.3 ± 4.6	31.0 ± 4.7	38.8 ± 5.4
$-\Delta V_{m,c}$ (μL/g)	39.8 ± 1.5	35.0 ± 1.7	29.0 ± 1.5	22.0 ± 1.6

expected at: $T_{max} \approx (T_g + T_m)/2$, with all three temperatures increasing with P.[53]

The effect of pressure on X_{cryst} is related to the crystal growth rate[54–57]:

$$\ln\dot{G}/\dot{G}_0 = C_1C_4T\left[C_2 + T - T_g(P)\right]^{-2} + C_3T_m(P)/\{T[T_m(P) - T]\}; \quad T_g \le T \le T_m \qquad (11)$$

where $C_1 = 900$ and $C_2 = 51.6$ are universal, C_3 is a nearly T-independent characteristic parameter and C_4 is adjustable. Differentiation of eq 11 indicates that depending on the pressure gradient of T_g and T_m the crystallization rate may be negative (as for polyolefins) or positive, as it is the case for PA-6.

The second additional parameter in eq 10, $\Delta V_{m,c}$, is the excess specific volume displayed in Figure 9. It has three contributions: the melting region volume change shown in Figure 6, ΔV_m, the least-squares shift of volume evident in Figure 7, and the volume change during annealing, $\Delta V_{ann} < 0$; the pressure dependence of the latter quantity is shown in Figure 10. As expected, the maximum annealing occurs during the initial heating and compressing.

In conclusion, the new analysis of the *PVT* behavior at $T_g \le T \le T_m$ separates the volume changes of the crystalline and liquid phase. This offers a reasonable description of the dynamics of crystallization and volume changes expressed by X_{cryst} and ΔV_{ann} versus P dependencies.

The Thermal Expansion and Compressibility Coefficients

One of the most interesting aspects of crystallization and melting appears in their compressibility and the thermal expansion coefficients of the semicrystalline polymers. Using the definitions in eq 1, the coefficients were calculated by two methods: (1) differentiating the experimental ln$V$ versus. P or T using the MicroMath Scientist Stineman's moving arch subroutine, and (2) by fitting the interpolated ln$V$ data (at constant T or P) to a

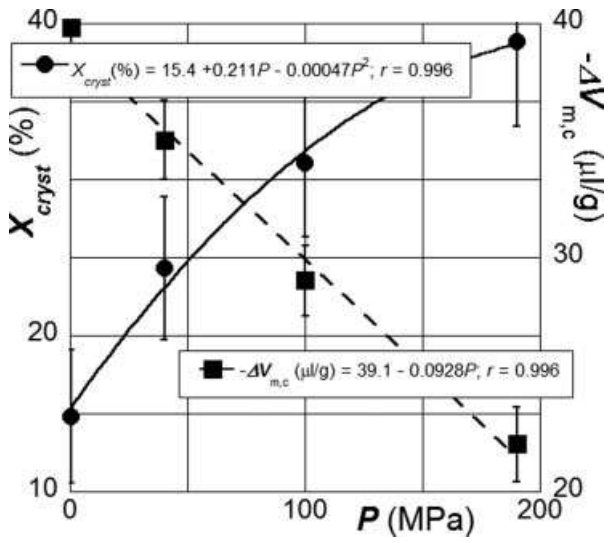

Figure 9. Pressure dependence of the total crystallinity, X_{cryst} (wt %), and excess specific volume, $-\Delta V_{m,c}$, for PA-6 (1022B).

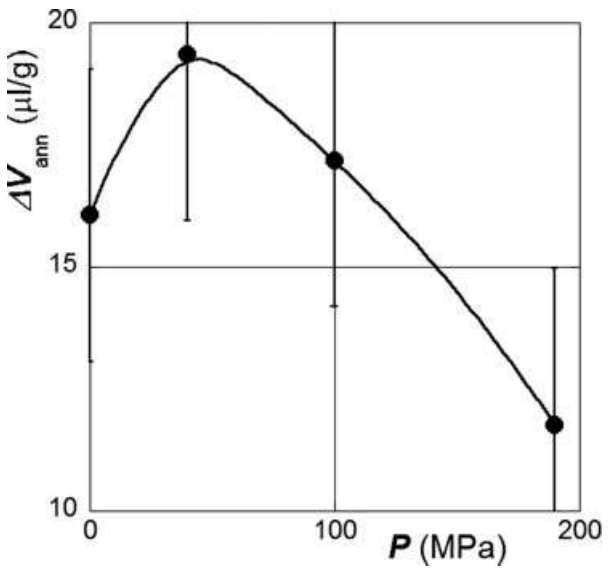

Figure 10. Pressure dependence of the annealed specific volume, ΔV_{ann}, for PA-6 (1022B).

polynomial function of P or T and then differentiating the latter. The first procedure involves local differentiation of all sets of data by the Stineman procedure, whereas the second separately fits the molten and solid phase data to a polynomial and then differentiates the empirical equations. Comparison of the results for κ and α coefficient is presented in Figures 11 and 12, respectively; for clarity only four isobars are shown. Note that the Stineman differentiation has a bias near the beginning and end of smooth data changes—only the results away from these are reliable. Both procedures show a dramatic reduction of $\alpha = \alpha(T)$ just above the melting zone, absent in the $\kappa = \kappa(T)$ dependence.

Because Figures 11 and 12 show consistent results of the two differentiation methods, the coefficients α and κ of PA-6 were calculated using the second procedure and the results are displayed in Figures 13 and 14, respectively. The comparative behavior of these functions is surprising, as there is a large difference of the T-behavior for α and κ —while the former shows a dramatic change of value across the melting zone, the latter increases with similar functional dependence in the solid and molten phase.

Before proceeding further, it was important to check if the observed difference of α and κ behavior takes place in other semicrystalline polymers. First analyzed was PA-6 *Capron-8200* from the

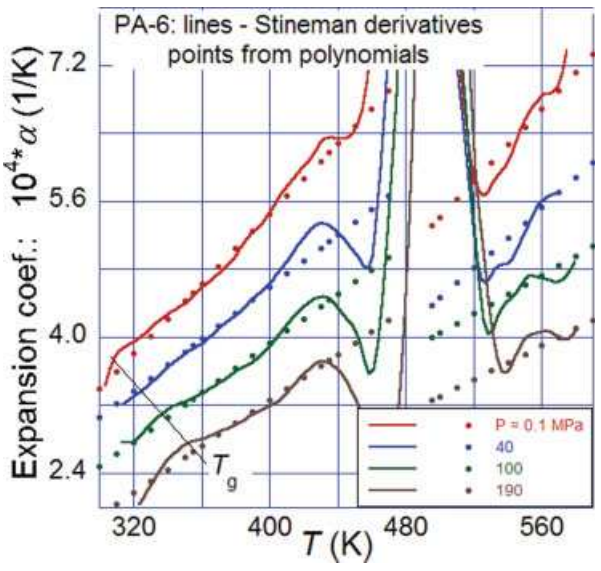

Figure 11. Thermal expansion coefficient of PA-6 versus T obtained by: (lines) the Stineman's procedure and (points) by differentiating the second order polynomials fitted separately to solid and molten phases. The glass transition, T_g, is also indicated.

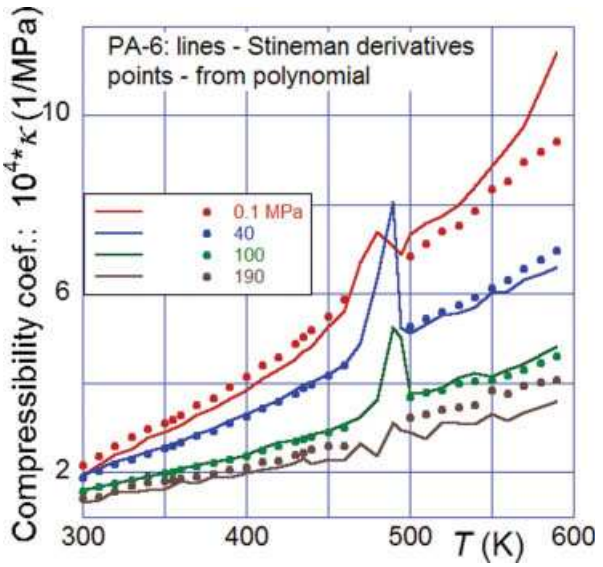

Figure 12. Compressibility coefficient of PA-6 versus T obtained by: (lines) the Stineman's derivatives and (points) by differentiating the second order polynomials fitted separately to solid and molten phases.

PVT data published by Zoller and Walsh (ref. no. D6098).[26] The computed coefficients showed quite similar dependencies as those in Figures 13 and 14. Next, κ and α coefficients of low density PE (LDPE, ref. no. D2040)[26] were computed (see Fig. 15)—here even stronger difference of the α and κ temperature behavior was obtained than that of PA-6. By contrast, α and κ of a random propylene-ethylene copolymer (Pro-fax SR256*M*) and that of polypropylene (Profax 6523, ref. no. D0394)

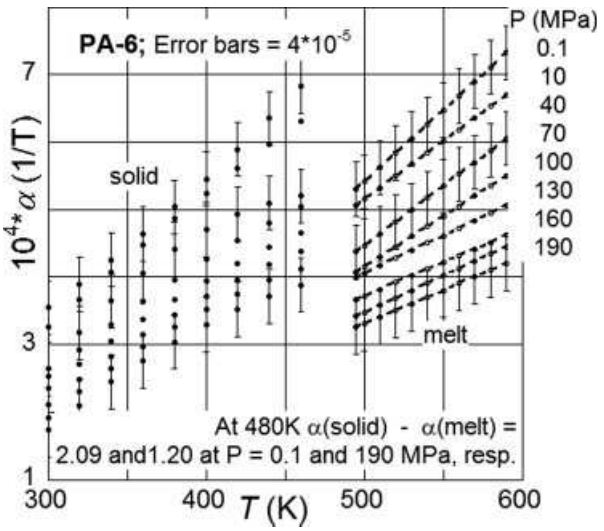

Figure 13. Thermal expansion coefficient of PA-6 1022B versus T at indicated pressures, P = 0.1–190 MPa.

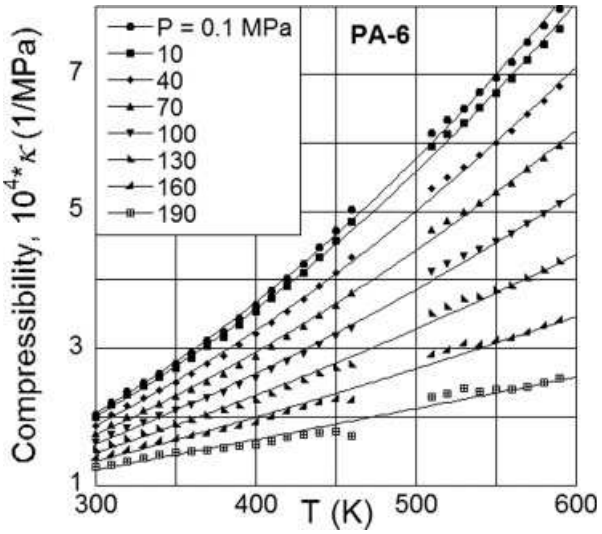

Figure 14. Compressibility coefficient of PA-6 1022B versus T at indicated pressures, P = 0.1–190 MPa.

showed similar T-dependence of both parameters on both sides of the T_m zone, without the α-discontinuity. In short, the α and κ behavior of semicrystalline polymers depends on the chemical nature, hence on the dominant helical structure on both sides of T_m.

According to eq 1, the coefficients α and κ represent the relative volume change, $\Delta V/V$, caused by T or P, keeping constant P and T, respectively. In the case of multi-phase system, as the one existing below T_m, one may assume that the macroscopic coefficient comprises contributions from both phases, proportional to their volume fractions, for example:

$$\alpha(P,T) = \sum \phi_i \alpha_i(P,T) = \alpha_{melt}\phi_{melt} + \alpha_{cryst}\phi_{cryst}; \quad P = \text{const}$$

$$\kappa(P,T) = \sum \phi_i \kappa_i(P,T) = \kappa_{melt}\phi_{melt} + \kappa_{cryst}\phi_{cryst}; \quad T = \text{const}$$

$$\phi_{melt} = 1 - \phi_{cryst} = \left[1 + \frac{\rho_{melt} X_{cryst}}{\rho_{cryst}(100 - X_{cryst})}\right]^{-1} \tag{12}$$

The relation suggests that at $T < T_m$ the PA-6 behavior should be dominated by melt:

$$\phi_{melt} \gg \phi_{cryst} \text{ as } (100 - X_{cryst})/\rho_{melt} \gg X_{cryst}/\rho_{cryst} \tag{13}$$

However, because the argument holds equally well for α as for κ, the observed different behavior must originate in the different effect of P and T on free volume and macromolecular configuration. For the molten state, this indeed was illustrated in Figures 1 and 2. At low free volume content, that is, at low T, κ changes little in comparison to α. Thus, low variability of κ, combined with inequality 13 may explain the effect illustrated in Figure 14.

The dependence $\alpha = \alpha(T)$ in Figure 13 shows a similar slope on both sides of the melting zone, with a step-decrease at T_m. Evidently, at $T < T_m$ two processes take place: thermal expansions of

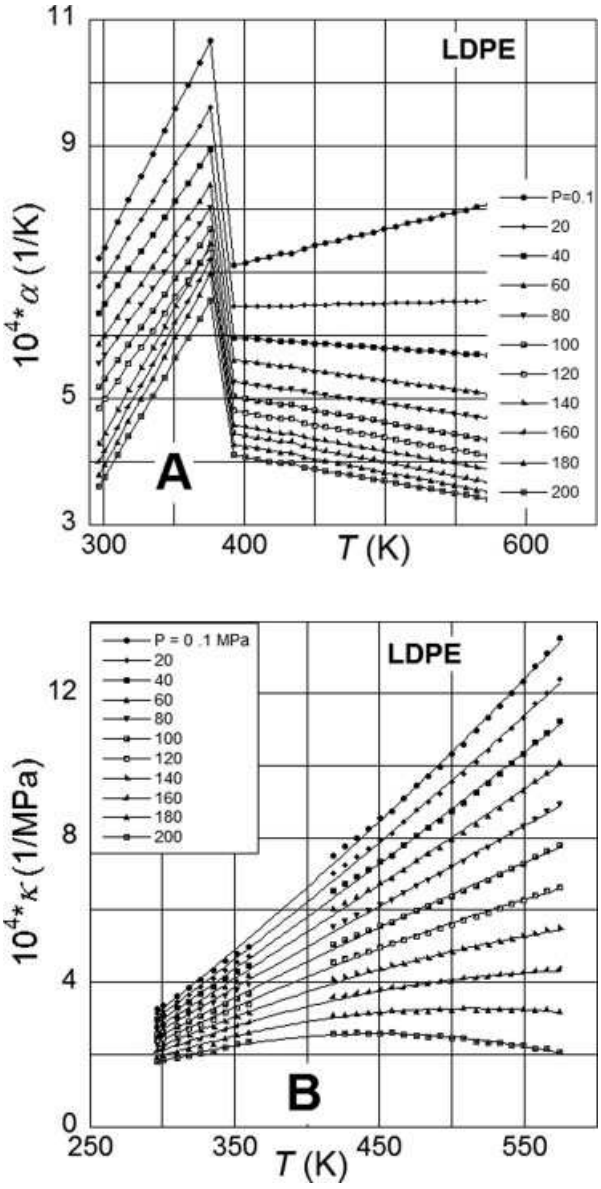

Figure 15. Thermal expansion coefficient (A) and compressibility coefficient (B) for LDPE. Data from ref. 26.

the solid and molten phase, as well as premelting of crystals. It is the latter that causes the $d\alpha/dT$ gradient to be larger below T_m than above. This mechanism may also be used for the interpretation of even more unexpected behavior of LDPE α and κ in Figure 15.

SUMMARY AND CONCLUSIONS

Polyamide-6 1022B from Toyota was studied in the solid and molten state at $T = 300$–600 K and $P = 0.1$–190 MPa. Its *PVT* behavior in the molten and solid state was measured following the isothermal standard procedure, scanning all P-levels before increasing T to the next level. The total run time of a single experiment was 23 to 45 h. The results were analyzed using the Simha-Somcynsky (S-S) equation of state (eos) for the melt and Midha-Nanda-Simha-Jain (MNSJ) eos for the crystalline phase. In the molten state the theoretical description provided excellent fit to the *PVT* surface with $\pm$ 0.0003 mL/g residuals of the specific volume, yielding the characteristic reducing parameters, P^*, V^*, T^*, the L-J interaction parameters, ε^* and v^*, as well as the free volume function, $h = h(V, T)$.

The *PVT* discontinuity in the melting region was characterized by three parameters: T_m, ΔT_m, and ΔV_m—the latter measuring the width and height of the first order transition. All three depend on P, as expected, T_m increased with P, whereas the two others decreased. Although the T_m value at ambient P was comparable to the values cited by literature, its pressure gradient was significantly lower than that reported for isobaric crystallization. Apparently, the pressure dilatometer detected constant volume before PA-6 reached maximum crystalline morphology.

For PA-6, the glass transition is weak and vitreous region starts at the relatively low temperature, $T_g = 316 \pm 2$ K, increasing with P at low rate of 0.1 K/MPa. In consequence, the solid-state data were only analyzed within the temperature range $T_g \leq T \leq T_m$ where two phases coexist—crystalline solid dispersed in liquid PA-6. During the *PVT* measurements, there is continuous change of the dynamic equilibrium between these phases, related to crystal annealing, pressure crystallization and premelting in the vicinity of the T_m region.

It has been found that the MNSJ theory cannot correctly reproduce the observed behavior in the solid state, for example, the predicted isobaric volume increase with T is smaller than observed (this behavior is in contrast with that reported by the authors for polyethylene). As a result, the solid-state *PVT* data were analyzed assuming that the behavior is a consequence of additive changes of the two phases, crystalline and molten; this approach leads to a reasonable description of the recorded data for PA-6.

In addition to the fundamental analysis of the *PVT* data, the derivative functions, the thermal expansion coefficient, $\alpha = \alpha(T, P)$, and the compressibility coefficient, $\kappa = \kappa(T, P)$, were computed. For PA-6, these two functions show surprisingly different behavior, while the isobaric values of κ increased in the solid and molten phase seemingly following the same, nearly linear dependence, α was discontinuous at the melting region, having higher values below T_m than above. The mechanism responsible for such behavior may be related to the free volume increase caused by premelting. The statistical thermodynamics of the liquid state predicts that α should be significantly more sensitive to free volume than κ.

This article was inspired by numerous discussions with R. Simha on the fundamental differences in the thermodynamic behavior of polymeric systems in the molten and solid state. Help of A. Usuki in obtaining PA-6 and its CPNC is gratefully acknowledged.

NOMENCLATURE

CPNC	Clay-containing polymeric nanocomposites
DSC	differential scanning calorimeter
eos	equation of state
L-J	Lennard-Jones
L-JD	Lennard-Jones and Devonshire
MNSJ	Midha-Nanda-Simha-Jain cell eos of crystalline phase
PA-6	poly(ε-caprolactam)
PE	polyethylene
PS	polystyrene
PVT	pressure-volume-temperature dependence
S-S	Simha-Somcynsky cell-hole theory or eos
$\dot{G}$	crystallization rate
$3c$	the external volume-dependent degrees of freedom per macromolecule
A_i, B_i	Lattice constants
B	bulk modulus
CD	coefficient of determination

C_i	parameters of eq 11
C_p	heat capacity at constant P
E	Tensile modulus
F	Helmholtz free energy
h	free volume parameter in S-S eos; $h = h(V, T)$
$M_s = M_n/s$	molecular weight of statistical segment
M_n, M_w	number- and weight-average molecular weight
P, P^*, P^0	pressure, the characteristic P-reducing parameter and solidification P
q	rate of vitrification by either cooling or compressing
R	the gas constant
r^2	correlation coefficient squared
s	number of statistical segments per macromolecule
s_p	dimensionless spread factor
t	Time
T, T^*	temperature and the characteristic temperature reducing parameter
T_c, T_g	crystallization and glass transition temperature
T_m	melting point
T_{max}	temperature at which the crystallization rate is the highest
T^0	solidification temperature
v^*	L-J segmental repulsion volume per statistical segment
V, V^*	specific volume and the characteristic volume reducing parameter
V_{solid}, V_{melt}	specific volume of the crystalline and liquid part at $T < T_m$
w	water content (wt %)
X_{cryst}	crystallinity content (wt %)
y	occupied volume fraction in S-S eos; $h = 1-y$
$z = 12$	coordination number
zq	the number of interchain contacts in a lattice; $zq = s(z-2) + 2$
ε^*	L-J maximum attractive energy
σ	standard deviation
ΔT_m	width of the melting zone
ΔV_{ann}	volume change caused by annealing
ΔV_m	volume change within melting zone
$\Delta V_{m,c}$	additional volume change in eq 10
α	thermal expansion coefficient
ϕ	volume fraction
γ_G	Grüneisen parameter
η	viscosity
κ	compressibility
ν	characteristic crystal frequency
θ	characteristic frequency function
ρ	density
Tilde	Indicates reduced variables, for example, as defined in eq 4.

REFERENCES AND NOTES

1. Moulinié, P.; Utracki, L. A. Polymer Physics, Chapter 6; Wiley: New York, 2009.
2. Lennard-Jones, J. E.; Devonshire, A. F. Proc Roy Soc 1937, 163, 53–70.
3. Prigogine, I.; Bellemans, A.; Naar-Colin, C. J Chem Phys 1957, 26, 710 and 751.
4. Peek, H. M.; Hill, T. L. J Chem Phys 1950, 18, 1252–1255.
5. (a) Simha, R.; Somcynsky, T.; Macromolecules 1969, 2, 342–350; (b) Somcynsky, T.; Simha, R. J Appl Phys 1971, 42, 4545–4548.
6. Simha, R.; Roe, J. M.; Nanda, V. S. J Appl Phys 1972, 43, 4312–4317.
7. Schell, W. J.; Simha, R.; Aklonis, J. J. J Macromol Sci 1969, A37, 1297–1313.
8. Midha, Y. R.; Nanda, V. S. Macromolecules 1977, 10, 1031–1035.
9. Simha, R.; Jain, R. K. J Polym Sci: Polym Phys Ed 1978, 16, 1471–1489.
10. Jain, R. K.; Simha, R. J Polym Sci: Polym Lett Ed 1979, 17, 33–37.
11. Jain, R. K.; Simha, R. J Polym Sci: Polym Phys Ed 1979, 17, 1929–1946.
12. Utracki, L. A. J Polym Sci Part B: Polym Phys 2008, 46, 791–805.
13. Utracki, L. A. J Polym Sci Part B: Polym Phys 2007, 45, 270–285.
14. Utracki, L. A.; Simha, R. Macromol Chem Phys Mol Theory Simul 2001, 10, 17–24.
15. Warfield, R. W.; Kayser, E. G.; Hartmann, B. Macromol Chem 1983, 184, 1927–1935.
16. Barker, R. E., Jr. J Appl Phys 1963, 34, 107–116.
17. Barker, R. E., Jr. J Appl Phys 1967, 38, 4234–4242.
18. Wada, Y.; Itani, A.; Nishi, T.; Nagai, S. J Polym Sci Part A: Polym Phys 1969, 7, 201–208.
19. Broadhurst, M. G.; Mopsik, F. I. J Chem Phys 1970, 52, 3634–3641.
20. Broadhurst, M. G.; Mopsik, F. I. J Chem Phys 1971, 54, 4239–4246.
21. Hofmeister, A. M.; Mao, H.-K. PNAS Geophys 2002, 99, 559–564.
22. Kulkarni, R. G.; Abd-Elmeguid, M.; Bukshpan, S.; Milants, K.; Verheyden, J.; Pattyn, H. Phys Status Solid B 1996, 193, 335–339.

23. Cui, G.-L.; Yu, R.-L. Phys B: Condens Matter 2007, 390, 220–224.
24. Pastine, D. J. J Chem Phys 1968, 49, 3012–3022.
25. Pastine, D. J. J Appl Phys 1970, 41, 5085–5087.
26. Zoller, P.; Walsh, D. Standard Pressure-Volume-Temperature Data for Polymers; Technomic Pub. Co.: Lancaster, Basel, 1995.
27. Utracki, L. A.; Lyngaae-Jørgensen, J. Rheol Acta 2002, 41, 394–407.
28. Simha, R.; Utracki, L. A.; Garcia-Rejon, A. Compos Interface 2001, 8, 345–353.
29. Utracki, L. A.; Simha, R.; Garcia-Rejon, A. Macromolecules 2003, 36, 2114–2121.
30. Utracki, L. A. Polymer 2005, 46, 11548–11556.
31. Schwarz, G. Cryogenics 1988, 28, 248–254.
32. Kazaryan, L. G.; Zezina, L. A.; Pavlov, N. N. Vysokomol Soed 1987, A29, 949–954.
33. Jain, A.; Vijayan, K. Curr Sci 2000, 78, 331–335.
34. Li, Y.; Goddard, W. A., III. Macromolecules 2002, 35, 8440–8455.
35. Vettegren, V. I.; Slutsker, A. I.; Giliarov, V. L.; Kulik, V. B.; Titenkov, L. S. Fizika Twerdogo Tela 2003, 45, 1528–1534.
36. Khanna, Y. P.; Kuhn, W. P.; Sichina, W. J. Macromolecules 1995, 28, 2644–2655.
37. Andrews, R. J.; Grulke, E. A. In Polymer Handbook, 4th ed.; Brandrup, J.; Immergut, E. H.; Grulke, E. A., Eds.; Wiley: New York, 1999.
38. Segal, L. Polym Eng Sci 1979, 19, 365–372.
39. Dlubek, G.; Redmann, F.; Krause-Rehberg, R. J Appl Polym Sci 2002, 84, 244–255.
40. Yoon, P. J.; Fornes, T. D.; Paul, D. R. Polymer 2002, 43, 6727–6741.
41. Khanna, Y. P.; Kuhn, W. P. J Polym Sci B: Polym Phys 1997, 35, 2219–2231.
42. Vettegren, V. I.; Titenkov, L. S.; Bronnikov, S. V. J Therm Anal 1992, 38, 1931–1045.
43. Liu, X.; Wu, Q. Polymer 2002, 43, 1933–1936.
44. Ramesh, C.; Bhoje-Gowd, E. Macromolecules 2001, 34, 3308–3313.
45. Bureau, M. N.; Denault, J.; Cole, K. C.; Enright, G. D. Polym Eng Sci 2002, 42, 1897–1906.
46. Ermolina, A. V.; Zezina, L. A.; Igonin, L. A. Mekhanika Polim 1968, 4, 200–204.
47. Zoller, P.; Fukhreddine, Y. A. Thermochim Acta 1994, 238, 397–415.
48. Kojima, Y.; Takahara, M.; Matsuoka, T.; Takahashi, H. J Appl Polym Sci 2001, 80, 1046–1051.
49. Gogolewski, S.; Pennings, A. J. Polymer 1973, 14, 463–464; *ibid*. 1975, 16, 673–679; *ibid*. 1977, 18, 647–653; *ibid*. 1977, 18, 654–659.
50. Brucato, V.; Crippa, G.; Piccarolo, S.; Titomanlio, G. Polym Eng Sci 1991, 31, 1411–1416.
51. Kojima, Y.; Usuki, A.; Kawasumi, M.; Okada, A.; Fukushima, Y.; Karauchi, T.; Kamigaito, O. J Mater Res 1993, 8, 1185–1189.
52. Fornes, T. D.; Paul, D. R. Polymer 2003, 44, 3945–3961.
53. La Carrubba, V.; Brucato, V.; Piccarolo, S. Polym Int 2004, 53, 61–68.
54. Takayanagi, M.; Kasumoto, N. Kogyo Kagaku Zasshi 1959, 62, 587.
55. Wei, K.-Y.; Cuculo, J. A.; Ihm, D. W. J Polym Sci: Polym Phys Ed 1983, 21, 1091–1101.
56. Ito, H.; Minagawa, K.; Takimoto, J.; Tada, K; Koyama, K. Colloid Polym Sci 1995, 273, 811–815.
57. Ito, H.; Tsutsumi, Y.; Minagawa, K.; Takimoto, J.; Koyama, K. Int Polym Process 1996, 11, 363–368.